

Enabling Integrated AI Control on DIII-D: A Control System Design with State-of-the-art Experiments

A. Rothstein,^{1, 2, a)} H.J. Farre-Kaga,^{1, 2, 3} J. Butt,² R. Shousha,³ K. Erickson,³ T. Wakatsuki,⁴ A. Jalalvand,² P. Steiner,² S.K. Kim,³ and E. Kolemen^{2, 3, b)}

¹⁾*The two authors contributed equally to this paper*

²⁾*Princeton University, Princeton, NJ, USA*

³⁾*Princeton Plasma Physics Laboratory, Princeton, NJ, USA*

⁴⁾*National Institutes for Quantum and Radiological Science and Technology, Naka, Japan*

We present the design and application of a general algorithm for Prediction And Control using MAchiNe learning (PACMAN) in DIII-D. Machine learning (ML)-based predictors and controllers have shown great promise in achieving regimes in which traditional controllers fail, such as tearing mode free scenarios, ELM-free scenarios and stable advanced tokamak conditions. The architecture presented here was deployed on DIII-D to facilitate the end-to-end implementation of advanced control experiments, from diagnostic processing to final actuation commands. This paper describes the detailed design of the algorithm and explains the motivation behind each design point. We also describe several successful ML control experiments in DIII-D using this algorithm, including a reinforcement learning controller targeting advanced non-inductive plasmas, a wide-pedestal quiescent H-mode ELM predictor, an Alfvén Eigenmode controller, a Model Predictive Control plasma profile controller and a state-machine Tearing Mode predictor-controller. There is also discussion on guiding principles for real-time machine learning controller design and implementation.

I. INTRODUCTION

Magnetic confinement fusion has the potential to provide sustainable, carbon-free energy to meet an increasing global energy demand. Among candidate reactor designs, the tokamak is considered one of the most promising for near-term commercialization⁹. Because tokamak plasmas are inherently dynamic, real-time feedback control is essential for achieving and maintaining advanced operational regimes in devices such as ITER³², DEMO⁷⁵, and SPARC¹⁷. The design of real-time plasma control systems (PCS) has therefore been the subject of sustained development across multiple devices^{17, 18, 20, 28, 31, 41, 43, 44, 55, 73, 74}.

Plasma instabilities evolve on a wide range of timescales, from the millisecond order for vertical displacement events (VDEs)³³ to over a hundred milliseconds for profile control. To address these requirements, modern PCS architectures employ multiple CPU cores operating at different cycle times, each dedicated to specific control objectives^{31, 44}. A key component of nearly all PCS systems is a real-time equilibrium reconstruction which provides the plasma shape and boundary information needed for fast position and shape control^{26, 46}.

The field of plasma physics has seen a surge in applications of machine learning (ML) across a wide range of tasks³ including ML for real-time control. One common approach is to develop surrogate models of computationally expensive physics codes^{30, 39, 47, 50, 51, 62, 63, 67} which is then integrated with conventional controllers. Beyond surrogates, ML methods have been applied to instability suppression and avoidance and profile prediction and control^{1, 11, 27, 29, 35, 37, 45, 48, 49, 60}. These event prediction methods are typically coupled with basic event thresholding or finite state controllers. Finally, the current state-of-the-art ML controllers utilize reinforcement

learning (RL) trained in offline simulator environments before deploying in a test reactor environment^{12, 19, 21, 22, 64, 70}.

Despite these advances, most ML-based controllers have been implemented as stand-alone demonstrations. Little effort has been devoted to creating a common, real-time compatible framework that simplifies deployment across multiple and diverse control applications. This presents a barrier to scaling ML-based control beyond one-off projects.

This work introduces such a framework, shown in Figure 1, called PACMAN (Prediction And Control using MAchiNe learning), and reports its first implementation on DIII-D. PACMAN builds on lessons from a prior profile-control oriented workflow², addressing its limitations in scalability, clarity of model-controller separation, diagnostic integration (new diagnostic signals), and timebase management. The design emphasizes modularity, fault-tolerance, and flexibility, making it possible to accommodate a wide range of ML models and controllers. Although demonstrated in a CPU-based environment, the principles are sufficiently general to be extended to PCS workflows that include other hardware such as GPUs^{6, 36, 58, 59} and FPGAs^{42, 72}.

The remainder of this paper is organized as follows: Section II presents an overview of the PACMAN architecture and its design rationale. Section III describes five experimental applications implemented within this PACMAN framework on DIII-D. Finally, Section IV summarizes the contribution, its potential limitations and outlines future directions.

II. ALGORITHM DESIGN

The PACMAN algorithm is outlined in Figure 2 and consists of four blocks:

1. Diagnostic input pre-processing
2. Model block
3. Controller block

^{a)}Electronic mail: arothstein@princeton.edu

^{b)}Electronic mail: ekolemen@pppl.gov

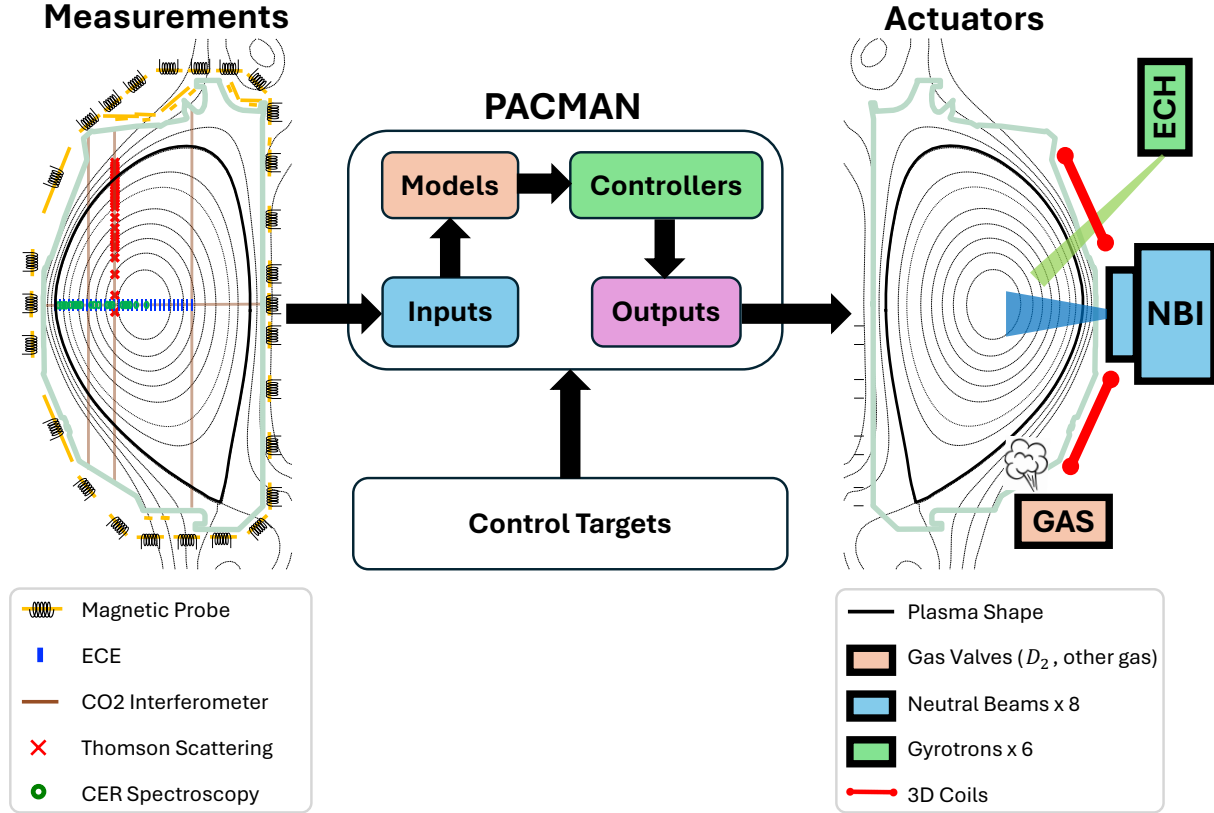


FIG. 1. DIII-D diagnostics, actuators and PACMAN. PACMAN receives diagnostic data and finds the optimal actuators to accomplish the user defined control targets. Location of diagnostics and actuators are approximate in this sketch.

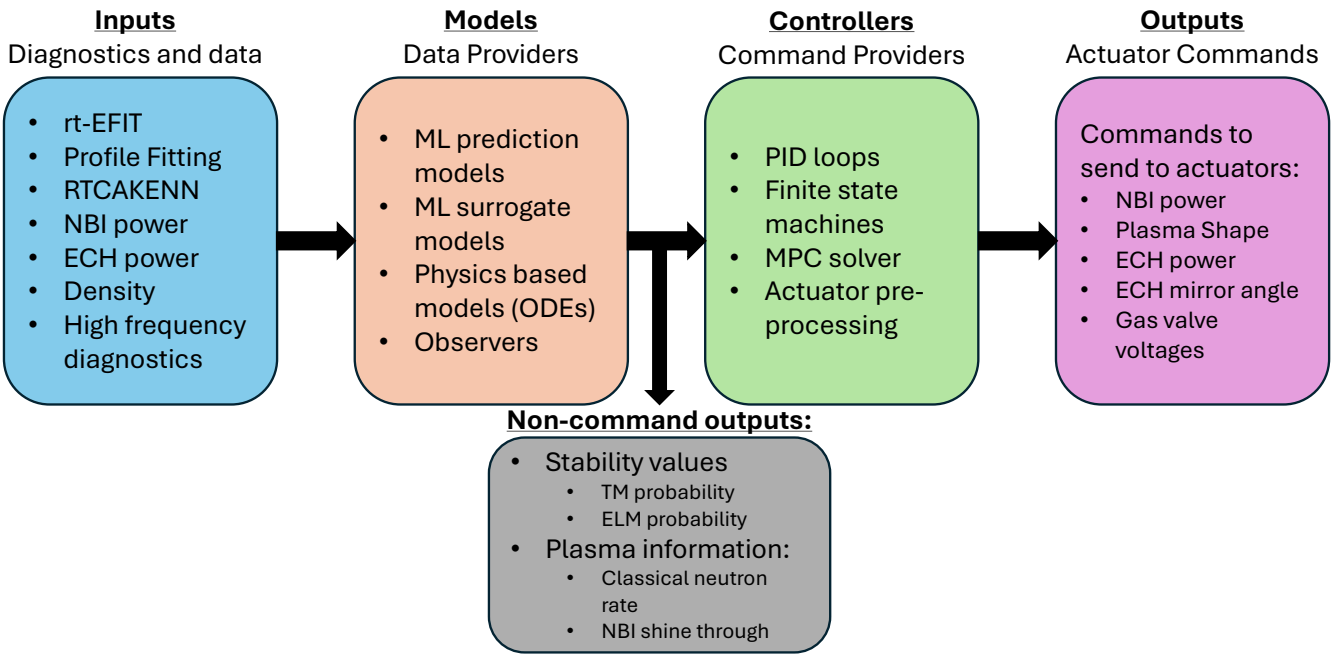


FIG. 2. General design of the PACMAN algorithm. The algorithm is an end-to-end controller, starting from diagnostic inputs, followed by ML, standard control, or physics-based models, then saving the ML outputs and sending the data to a controller such as finite state machines and PIDs, and ending with commands to actuators such as neutral beam injector (NBI) power, electron cyclotron heating (ECH) power, and gas requests.

4. Actuation output post-processing

While the subsequent subsections (Section II A, II B, II C, II D) will describe each block in detail, here we will explain the high level design decisions that went into the overall architecture.

The first key design principle is the separation of each block and the flow of data and information forward from one block to the next. The models can utilize any of the inputs, the controllers can utilize any data from the models and inputs, and finally the actuator block can utilize all preceding data. A key separation is that components within a block cannot communicate within the block. For example, models cannot communicate with other models and similarly controllers cannot communicate with other controllers. If a model needs the output of another model, these would be jointly considered a single model, with the same approach also applied to integrated controllers that need to communicate. Multiple controllers that have to interact would be considered a single “Controller”. This important requirement was made to avoid possible dependency collisions where some models must complete running before others can start. This enables a future option of running all models in parallel followed by all controllers in parallel, greatly speeding up the entire real-time pipeline. Error checking is centralized at block interfaces, reducing overhead and clarifying where faults are detected and handled.

The next key principle is the idea of a 3 level algorithm design. In this paradigm, algorithms are classified into 3 levels with distinct purposes and communicate with algorithms in adjacent levels. These levels are defined as:

1. **Level 1:** Lowest-level algorithms to calculate hardware commands from more generic actuator commands or directly process diagnostic data. Examples here include calculating exact power supply voltage requests from desired coil currents or reading digitizer voltages. A typical user will never interact with a Level 1 algorithm.
2. **Level 2:** Mid-level algorithms that process raw diagnostic data or turn high level actuator commands into lower level commands. Examples here include fitting Thomson scattering data to produce n_e profiles or computing On/Off modulations of NBIs. A typical user will have some interactions with a Level 2 algorithm.
3. **Level 3:** High-level algorithms that process data and compute high level actuator commands to achieve a desired control objective. Examples here include most standard control such as PID-based β_N control as well as more advanced controllers. A typical user should have the majority of their interactions with Level 3 algorithms.

This design closely mimics the human interaction in a typical tokamak control room. Teams of engineers own the actuators controlled by Level 1 algorithms. Physics operators, akin to a Level 2 algorithm, bridge the gap between experimentalists and the technical staff that operate the machine. Experimentalists nominally existing at Level 3 ask physics

operators to conduct experiments on their behalf. This separation of concern not only provides a metaphorical comparison between software and users but mimics the possible administrative constraints in the control room that allow effective tokamak operation. For example, a physics operator might tell an experimentalist that a particular plasma scenario is out of reach, and similarly a Level 2 algorithm may accept or reject a total beam power request based on configured limits.

While this is the design standard is not enforced as the standard for algorithm design on DIII-D, it was first introduced on the NSTX PCS and has been attempted to be used as a general design principle. Because of this, it is worth noting that this design principle does not hold across all algorithms in the DIII-D PCS and there are edge cases of algorithms crossing into 2 levels. PACMAN sits cleanly in Level 3 and takes control objectives from the user combined with processed data provided by Level 2 algorithms and calculates actuator commands that are sent down to Level 2 algorithms.

Moving towards discussion on each individual block, their individual design decisions were made to achieve the following major objectives:

- Scalable to many models and controllers where all can be run concurrently
- Agnostic to type of ML model or controller type
- Standard processing of inputs that is still flexible
- Rough cycle time goal of 5 – 50 ms range. All should run in this range even if they take performance hits
- Actuator arbitration and handling of conflicting actuator commands

A. Input Gathering and Pre-processing

The first block in PACMAN gathers and standardizes input data to further process it in the subsequent blocks. At the time of writing, the full list of real-time inputs at DIII-D is given in the top half of Table I. However, new diagnostics are constantly added to DIII-D while other currently offline-only diagnostics are made real-time capable as well. In order to use new diagnostics at different time scales, and data sizes, it is necessary to design the input block to be adaptable to new diagnostics.

Diagnostics run on timescales varying from high frequency (1 MHz) down to 100 Hz, or every 10 ms. Storing and buffering this quantity of data is intractable in a real-time system that is expected to function reliably. Note that this is not a problem for PACMAN specifically, but is an issue that any conventional real-time control system must deal with. We let PACMAN rely on the Level 2 data providers to handle the data buffering on their own CPUs and then read the latest buffer information. This streamlines the data collection process and improves PACMAN’s adaptability to new diagnostics by not needing to handle individual data buffering internally. PACMAN saves the most recent cycle of data, typically the previous 10 ms or 20 ms, to provide as reference for how the plasma

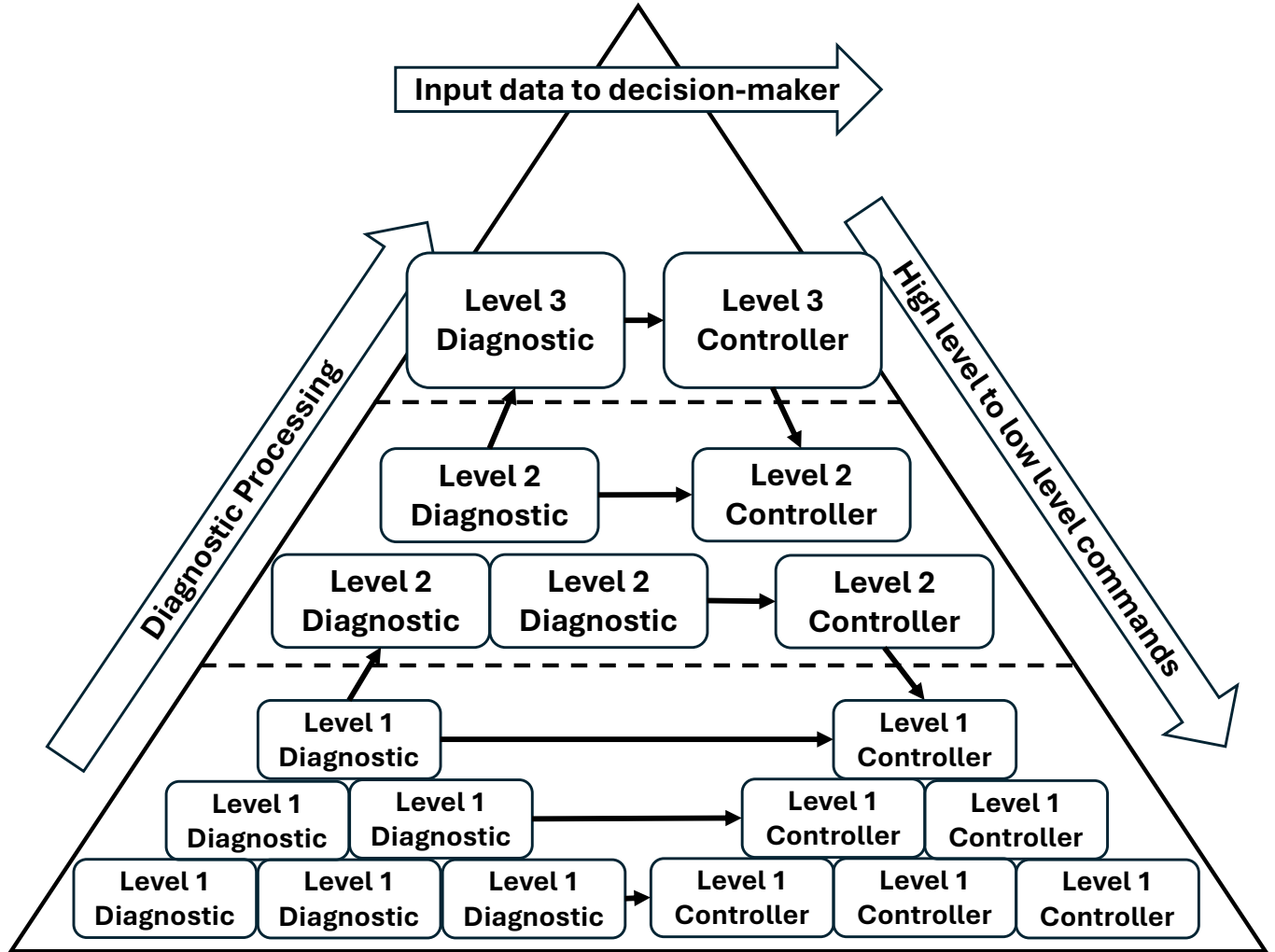


FIG. 3. 3 level design structure of the PCS diagnostics and algorithms. The flow of diagnostic information is always up levels and to the right, where raw diagnostic data is processed, then may be fed to automated fitting routines such as real-time EFIT²⁶, before being provided as inputs to various controllers. On the controller side, commands travel down the levels from the highest controllers, which may decide on target profile objectives, or plasma stability targets, and gets passed down to lower level controllers that will achieve those high level goals before the lowest level controllers calculate exact commands to be send to hardware. Of note, as seen in the figure there are typically more Level 1 diagnostics and controllers than there are Level 2 or 3. PACMAN is at the top of the pyramid as a Level 3 controller.

state is evolving. PACMAN does not save data over a longer time horizon because that is expensive in terms of complicating the PACMAN algorithm and expensive in terms of computational cost. The responsibility to buffer data is on any level 2 diagnostic to buffer relevant data and provide it to PACMAN's input block.

General pre-processing is kept as minimal as possible to leave ML models to interact with the data closest to the diagnostics. One of the major signal pre-processing computed is the low pass filtering of signals such as NBI power and torque, P_{NBI} and T_{NBI} , respectively, as well as ECH power, P_{ECH} , which achieve continuous power control by quickly alternating power on and off at fixed amounts. The toroidal field is approximated by taking the current from the B-coil ($I_{B_{coil}}$) and multiplying by a geometric factor for the DIII-D configuration of $B_T = \frac{144\mu_0}{2\pi \times 1.6955\text{m}} I_{B_{coil}}$. We do not normalize any

signals in a custom way, such as z or $(0, 1)$ normalization as it is required for ML models, because the exact method of custom normalization depends on the actual model. Thus, these kinds of data-dependent normalizations are part of the model block to maintain flexibility for every model to use the normalization methods that were found most suitable during the ML model development.

Additionally, the input block must check for real-time errors in all of the diagnostic signals and inform downstream models and controllers of diagnostic failures. These checks come in a variety of types and are specific to what is providing the data. In the case of real-time EFIT, there is a built-in error waveform to inform if the calculation converged. Other checks can involve checking if a temperature profile is greater than 0 or if the timestamp of the most recent diagnostic data is too old. These checks are important for two reasons: first they

Input	Source	Time Scale (ms)	Pre-processing
Plasma Shape Information	Real-time EFIT ²⁶	<1	
B_T	Rogowski coils	<1	
I_P	Rogowski coils	<1	
NBI power and torque	NBI Algorithm ⁵⁴	10	
ECH power	ECH Algorithm ¹⁰	10	
ECH mirror angles	ECH mirror encoders ⁴⁰	20	
ECH and ECCD deposition	Real-time TORBEAM ⁵⁶	20	
Real-time Kinetic Profiles	RTCAKENN ⁶⁷	5	
Average n_e	CO ₂ interferometer	1	
Current profile measurements	Motional Stark Effect ³⁴	10	
Ion temperature, density, and rotation profiles	Charge Exchange Recombination ¹⁵	20	Profile Fitting
Electron temperature and density profiles	Thomson Scattering ⁵⁷	20	Profile Fitting
Local n_e fluctuations	Electron Cyclotron Emission ⁴	0.001	
Global n_e fluctuations	CO ₂ Interferometer Fluctuations	0.001	
Turbulence Measurement	Beam Emission Spectroscopy	0.001	
Outputs	Source	Time Scale (ms)	Post-processing
NBI Power	VEP ⁷	10	LP Filter
NBI Torque	VEP ⁷	10	LP Filter
Individual NBI dutycycles	VEP ⁷	10	LP Filter
ECH power	Gyrotron Algorithm ¹⁰	10	LP Filter
ECH mirror angle	Real-time TORBEAM ^{40,56}	100	
Gas voltages	Gas Algorithm	1	
Shape targets	Proximity Control ⁵	1	
RMP Current	3D Field Algorithm ²³	1	
RMP Phasing	3D Field Algorithm ²³	1	
RMP n number	3D Field Algorithm ²³	1	

TABLE I. List of all inputs that can be used as model inputs within PACMAN and all possible output actuators. The timescales of inputs are how often new diagnostic data is received or processed by external algorithms, i.e. in the case of ion temperature profiles the 20 ms timescale is how often **Profile Fitting** computes new fitted profiles, not how often new diagnostic data is produced. The actuator timescales are based on how quickly actuator effects can affect the plasma. While ECH power can be turned on in a sub-millisecond timescale, to achieve continuous modulated power requires waiting closer to 10 ms to get a well time-averaged power.

provide a decision pipeline for models to decide if they will run without correct input data (usually they will not), and second, this provides insight in the control room that specific input data had issues during the last shot and must be addressed before the next shot. PACMAN is robust to diagnostic errors, so a model/controller will simply not run if an essential diagnostic is unavailable for that timestep.

In summary, the Input block in PACMAN provides error-checked real-time data that has been gathered from Level 2 algorithms as well as the data from the previous cycle. There is minimal pre-processing to maximize flexibility of the models in the next block.

B. Model Block

The next section in the PACMAN algorithm is the model block. This is where any typical ML model will cover tasks that involve taking data from the input block and producing values actionable by the controller block. To be clear, for the applications mentioned here we describe the use of ML models in this block, but this block can execute non-ML models that meet the requirements to function here.

Every model block receives input/output information as well as custom parameters for normalization and standardiza-

tion of the input data, information about the model such as the model type and the number of models. Every model block runs through the following steps:

1. All information is passed to the model block via a structured data format that needs to be parsed task-dependently.
2. The input data is preprocessed. This involves custom pre-processing steps like filtering/smoothing and normalization.
3. The actual ML model is instantiated. Since PACMAN is designed model-agnostic, a wide range of implementations of ML models is supported. Several ML models and functions may be run in series within the model block.
4. All the errors produced from the input block are evaluated to make sure the input data is valid. Only if this is successful, the subsequent steps are executed in order to provide machine protection for the tokamak.
5. The preprocessed input data is passed through the ML model and the raw outputs are collected.

6. The raw outputs are customly post-processed. This can again involve smoothing/filtering, or also thresholding for binary tasks.
7. The post-processed output is written back into the structured data format such that the subsequent controller block can parse it.

Within PACMAN, we support a large variety of ML models. Currently, this includes: ML surrogate models, event prediction models, plasma profile prediction models, observers, latent space mappings, or RL models. More models for new tasks are steadily integrated. It is important to note the flexibility of PACMAN in the sense that all models are responsible for handling their custom normalizations and any model-specific processing of inputs before running the specific model.

Currently, PACMAN supports multiple implementations for ML models in real-time such as `keras2c`¹⁶, PCAnet⁵⁰, reservoir computing networks (RCN)⁶², or more classical approaches with less ML such as linear regression models, random forests⁶, or standard mathematical functions. Within this structure, we have leveraged the flexibility to implement a more complex deep survival machine architecture⁵² to help with tokamak event prediction.

While `keras2c` provides an easy path to PCS model implementation, it does so at significant cost to stack memory use and does not scale well to many `keras2c`-generated functions running concurrently. This is mainly due to developer time constraints and this problem could in theory be solved with additional focused code development. Additionally, this limits the total size of a model that is implementable, with the limit of a DIII-D `keras2c`-generated function file being approximately 3 MB. The advantage of using `keras2c` is the ability to use more complex ML layers, such as convolutional layers and LSTMs, while other implementations that scale better by allocating memory on the heap rather than the stack, such as PCAnet, limit the user to just MLP architectures.

As described previously, all models in the model block are fully independent and may be run in series or parallel depending on computing hardware availability. While this limits the ability for models to contribute to inputs for other models, this decision enables the future ability to provide a significant computation speed-up by enabling parallelization. If a user desires some type of ML hierarchical model that wants to use outputs from multiple models, such a model could be implemented as multiple `keras2c`-generated functions within the same single Model sub-block. For example, the survival models mentioned are comprised of 4 `keras2c`-generated functions run as one Model.

The model block provides a variety of outputs to be used in the controller block or other parts of the PCS. The simplest are computed values needed by other algorithms external to PACMAN. Examples here could be surrogate models that calculate physics values such as NBI shine-through, MHD stability metrics, ECH ray trajectories, or plasma profile estimates. Those model outputs can also go directly to the controller block for basic control processing such as PID controllers, thresholding-based decision making, or finite state machines.

Other model block outputs can include outputs that require additional processing or advanced input processing for the specific controller such as an advanced plasma state mapping used in Section III E.

C. Controller Block

The controller block can be considered the ‘decision maker’ of the PACMAN algorithm. Each module in the controller block will receive the necessary outputs from the model block, as well as any required input block data, and calculate actuator commands to send to the output block. Again following the structure of the model block, none of the controllers can interact with any other controller within the controller block and any integrated controller would be a single “Controller” with multiple internal algorithms running. This enables future versions of PACMAN to parallelize controllers because they can all run independently.

This restriction on separation controllers may limit possible future integrated controllers, but have decided the limitations are worth the safety provided in avoiding possible conflicting actuator commands. Future applications that aim for more integrated control within PACMAN could turn on and off specific controllers based on what part of the shot is occurring. The user may utilize specific controllers in I_P flattop while others may be used during ramp-up and ramp-down sequences.

Example controllers can be finite state machines⁶⁵, basic thresholding decision making, PID control, MPC optimizers, other advanced control algorithms, or anything that will produce an actuator request from model outputs or diagnostic data. Each module in the controller block can provide any subset of possible actuators listed in Table I, and multiple controllers can attempt to control the same actuators. Collisions between actuator commands are handled within the outputs block.

A final note is the controllers are aware of previous real-time errors from inputs as well as models. If any of the inputs for a specific controller have an error, whether from the model block or input block, then the controller will not compute any actuator command. This is done to maintain machine safety in an abundance of caution, but of note sometimes inaction can potentially be more dangerous than a bad action. In the future, other default actions could be created such as designated ramp-down sequences to safely shutdown the plasma.

D. Actuator Output and Post-Processing

Finally the output block gathers commands from the controller block, imposes additional machine safety constraints, and sends commands to Level 2 algorithms to handle actuation. The list of PACMAN controllable real-time actuators on DIII-D, at present, is listed in the bottom half of Table I. Similar to the table of inputs, PACMAN has been designed to handle future new actuators being added in anticipation of advancements on DIII-D, for example shattered pellet injection. While some actuators can change quicker than PACMAN’s

millisecond evaluation timescale, PACMAN cannot send commands faster than it can run. This limits the speed at which new actuation commands can be given, but at the millisecond timescale that is sufficient for most plasma instabilities of interest. PACMAN would be inappropriate for controllers targeting events like VDEs which can evolve and disrupt on sub-millisecond timescales.

First, the output block checks for any actuator collisions from the different controllers. If the output block receives two conflicting actuator commands, no actuation is output to maintain machine safety, and the operators are informed of the controller actuation conflict. While this approach is naive at present, the separation and flexibility provided by the output block enable future improvements to actuator conflicts. Multiple controller actuation can be added together where one model provide a ‘base load’ for an actuator like P_{NBI} and another model provides a minor correction with some ΔP_{NBI} .

Finally before any commands are sent, final clamps on actuator commands are done to set the minimum and maximum values of the commands. While many of these safety limits exist at various lower levels the DIII-D PCS hierarchy, we include them here to guarantee that no bad actuator commands will be executed. This includes setting minimums and maximums for gas valve voltages, P_{NBI} , P_{ECH} , and limits to ECH mirror angles and 3D coil currents.

III. EXPERIMENTAL APPLICATIONS

In this section we will highlight some of the successful applications of the PACMAN algorithm for real-time plasma control. These applications are summarized in Table II. Each algorithm fits neatly into the block described in Section II by the visualization in Figure 4. While there are additional algorithms that have been deployed in experiment on the DIII-D PCS using the PACMAN framework, the examples given here highlight the flexibility of the architecture to enable deployment of various different ML model and controller types to achieve a diverse set of control objectives.

Each experiment described in this section will feature: a description of the model or controller objectives, the list of model inputs and outputs, and finally discuss what computations occur in the model and controller blocks, respectively.

A. Reinforcement Learning Controller

The first example controller is an RL based β_N and internal transport barrier (ITB) controller which demonstrates ‘full ML control’ where the outputs of an ML algorithm fully decide actuator commands, subject to hard coded machine safety actuator limits. This was originally trained for the DEMO reactor⁷⁰ and a similar RL controller was trained offline using the RAPTOR code²⁵ as a simulator environment. The control objectives were: follow a β_N target trajectory and excite ITBs in flattop in the high q_{min} advanced tokamak scenario. After offline training was completed, the hierarchical RL model was converted to 4 C functions using keras2c. For more details on

the controller and experimental results, look to Wakatsuki⁶⁹. Real-time time traces of some inputs, some model outputs, and final actuator commands can be seen in Figure 5.

The RL model was trained to take in the q and T_e profiles along with present actuator information. There was additional input pre-processing added to compute the magnetic shear, $s2 = 2 \frac{\psi_N}{q} \frac{dq}{d\psi_N}$, from the q profile and to calculate on and off axis NBI powers from individual NBI powers. The model block outputs request for $P_{NBI, on-axis}$, $P_{NBI, off-axis}$, and P_{ECH} . For the control objectives, this RL controller needed PACMAN to run at 50 ms cycle time and this was achieved.

The keras2c-generated functions were placed into the model block of PACMAN and given the appropriate inputs from the input block. The hierarchical structure used a first model to observe information about the ITBs and to produce an index to be used by the controller to decide which RL model function to use. Using this index, one of three keras2c-generated functions was selected to run. This secondary model took the same inputs as the observer and produced output signals of $P_{NBI, on-axis}$, $P_{NBI, off-axis}$, and P_{ECH} to be passed to the controller block for further processing.

The controller block for the RL ITB model took the outputs from the final keras2c-generated function and converted them to appropriate commands for the Level 2 algorithm in the PCS. The NBI control algorithm in the DIII-D PCS cannot receive targets for $P_{NBI, on-axis}$ and $P_{NBI, off-axis}$ directly, so the controller block was used to convert $P_{NBI, on-axis}$ and $P_{NBI, off-axis}$ to appropriate individual NBI powers to achieve those actuator target commands.

B. TM control with ECCD

The next controller utilized a real-time tearing mode (TM) predictor model to steer the ECH mirror and preemptively suppress TMs. This model was trained using the Auton Survival Model framework⁵² and the controller was tested experimentally in the elevated q_{min} advanced tokamak scenario. For a complete detailing of the ML model and control results, look to Rothstein et al.⁶¹ and Farre-Kaga et al.²⁴.

The inputs for the TM predictor model were the profiles provided by RTCAKENN, P_{NBI} , P_{ECH} , and various scalar parameters from rt-EFIT. The output of the controller block is an ECH mirror objective: a ρ aiming target for broad off-axis current drive or the $q = 2$ rational surface for TM suppression. With PACMAN sending one of these ECH mirror objectives, the Level 2 algorithms of the real-time TORBEAM combined with real-time ECH mirror steering can find the optimal ECH mirror angle to achieve the ECH mirror target. Due to slow actuation timescale of ECH mirror steering, the target inference time for this controller was under 10 ms and easily achieved by PACMAN.

The model block contains the C implementation of the Deep Survival Machine in the Auton Survival package with keras2c-generated functions. The internal math functions used were made real-time compatible and avoid any possible overflow errors from standard ML functions like LogSoftMax and LogSoftExp. The final output of the model block is a TM

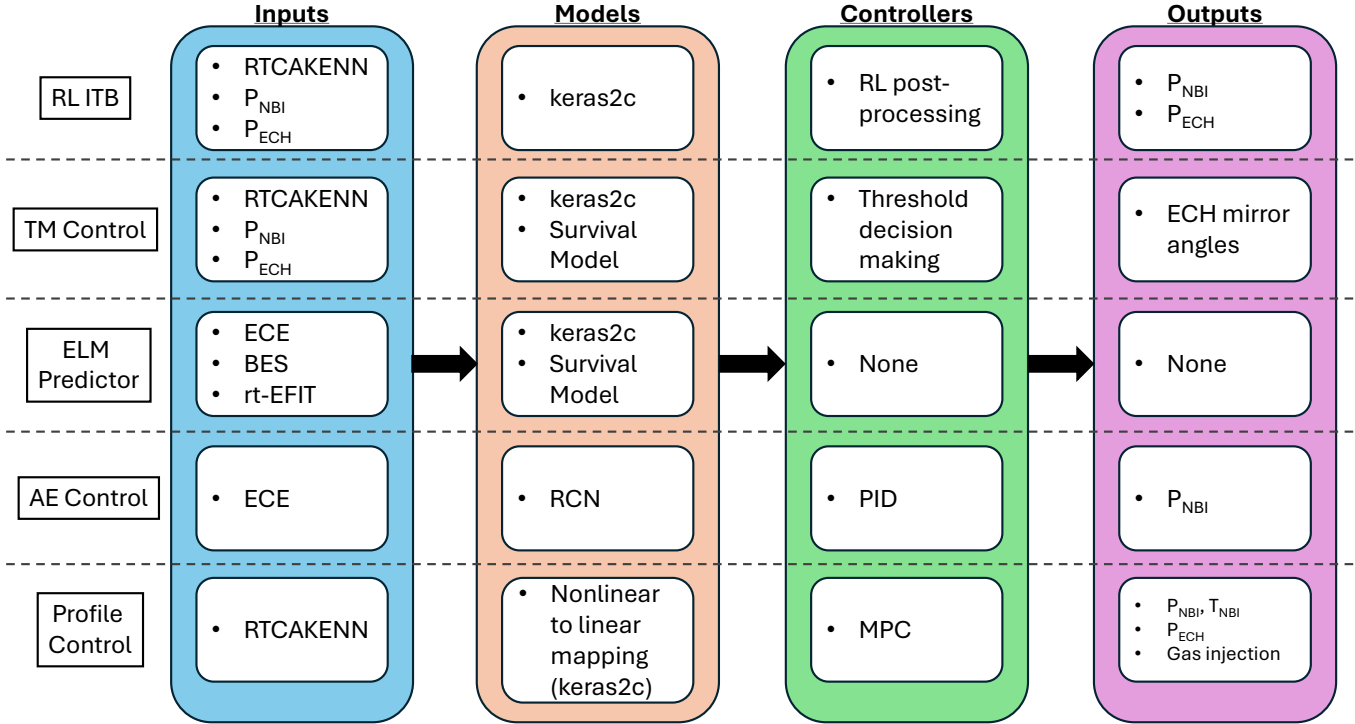


FIG. 4. Overview of the 5 experimental applications that are described. Each block is depicted mirroring the layout from Figure 2, where each horizontal dashed line separates each experiment. Note the many shared inputs and outputs that utilize the framework.

Model/Controller Type	Objective	Actuator	Inference Time (ms)
RL Controller	β_N and ITB Control	P_{NBI} and P_{ECH}	0.8
TM Controller	TM Avoidance	ECH mirror angle	0.6
ELM Predictor	ELM Prediction	None	0.2
AE Controller	Suppress AEs	P_{NBI}	0.65
Latent-linear MPC	P_{NBI} , T_{NBI} , P_{ECH} and gas injection		15

TABLE II. Overview of the 5 PACMAN experimental applications described in Section III. Each control type is listed along with the control objective, the actuators used, and the time scale of the ML model execution.

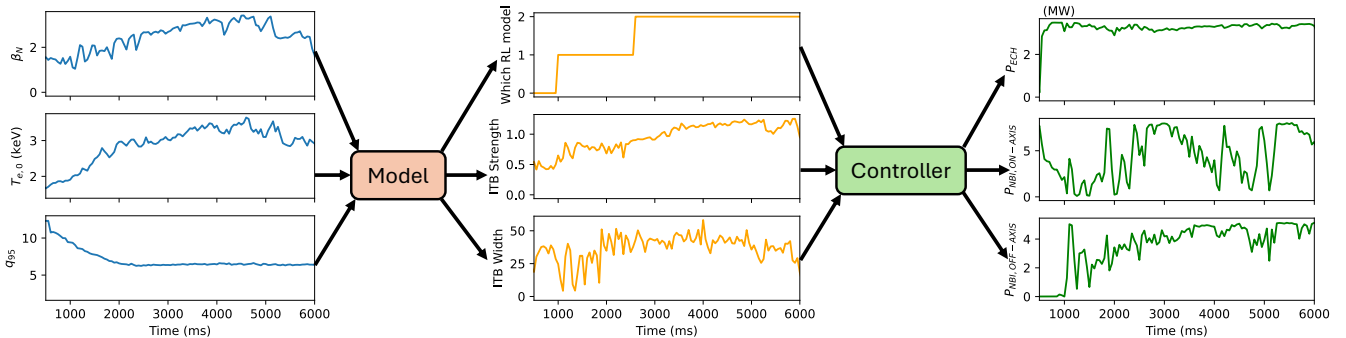


FIG. 5. DIII-D shot 204975 where the RL ITB controller was used to control β_N and ITBs. On the left are three of the real-time inputs: β_N , core electron temperature, and the q profile at $\psi_N = 0.95$. These along with the remaining inputs are fed into the model where the model outputs information on which RL model was selected as well as ITB strength and width. This information is fed into the controller block that finalizes the ECH, on-axis NBI power, and off-axis NBI power that get sent to the actuators.

probability over some time horizon, where the time horizon is a configurable user input.

Finally, the controller block of the TM controller uses a basic thresholding scheme to select gyrotron tasks, also referred to as a finite state machine. For example, when the TM probability rises above 10%, the first gyrotron will switch from off-axis current drive to $q = 2$ surface tracking. If the TM probability rises above 20%, then the second gyrotron will switch tasks and so on. There is also an additional low pass filter on the TM probability to smooth the signal and avoid changing the actuator significantly based on one possible poor data in a specific CPU cycle. Combining this control scheme with an ML predictor model enables a control scheme based on physics intuition of TM control, while leveraging advanced ML techniques to predict stability in real-time.

C. ELM Prediction

The third application example of this framework was in sporadic breakthrough ELM prediction in wide-pedestal QH mode (WPQH). Unlike the other applications, this example utilized the *non-command outputs* path to leverage PACMAN's out-of-the-box ready processing of real-time diagnostic data to plug into an already developed external controller. This model and controller were deployed and tested in an experiment for WPQH pedestal control, the details of which are presented in an upcoming paper by Butt et al.⁸.

Sporadic breakthrough ELMs in intrinsically ELM-free plasmas is a phenomenon not yet well understood from a physics perspective, so a simple predictive model does not yet exist. Since over a decade of WPQH experiments have been compiled on DIII-D, a machine-learning approach was taken to predict these ELMs. The complicated nature of this singular-event prediction task compelled us to utilize a wide-swath of diagnostics, including measurements of: turbulence (beam-emission spectroscopy [BES]), line-averaged density (CO_2 interferometry), local temperature gradients (electron-cyclotron emission [ECE]), D_α light emission, and actuator information from the neutral beams, ECH, and gas.

A deep survival machine learning model to predict sporadic breakthrough ELMs was trained offline with the Auton Survival Model framework⁵² using each of the aforementioned diagnostic measurements as input. Detailed documentation on the model, training, and database study is provided in an upcoming paper by Farre-Kaga et al.²⁴. The trained model was converted to 4 C functions using `keras2c`. As documented by Conlin et al.¹⁶, the outputted C functions are designed to be real-time compatible. Additional care was taken to ensure inputs provided to the `keras2c`-generated functions and internal math functions are bounded to avoid overflow. Based on the range of timescales of the prediction and control tasks, spanning the model's median prediction time of ~ 100 ms and the model's execution time of $\sim 200\mu\text{s}$, a short CPU cycle time of 2 ms was selected. The output from the model block is (1-survivability), which represents the likelihood of ELM-free termination over a user-configurable time-horizon. The model block output is provided to the ELM-free PCS cat-

egory's ELM avoidance algorithm, which conducts actuator decision-making.

For integrated testing, the model block also features a user-configurable debug waveform, which can be toggled to override the ML-model prediction to conduct integrated tests for inter-PCS algorithm communication and controller-side prediction handling.

D. Alfén Eigenmode Controller

An ML-based Alfén Eigenmode (AE) detection model was trained to classify different types of AEs based on ECE data^{38,62}. This observer model is an RCN-based ML model and was combined with basic proportional control (P-control) of P_{NBI} to directly control the presence of AEs. This controller was tested and deployed in the ramp-up of a DIII-D shot where AEs are typically observed.

The inputs for the AE detection model are purely ECE data. As shown in Jalalvand et al.³⁸, the performance of the model is generally stable to the frequency of data and so we receive data at the CPU cycle time on the order of 1 ms, or 1 kHz. The ECE data is received at 1 MHz and is down-sampled without impacting the accuracy of the model. The output of the controller is P_{NBI} and because NBI power directly affects the energetic particle distribution, this actuator will directly affect the AE amplitudes. The target CPU cycle time was approximately 5 ms as that about the minimum timescale to change P_{NBI} and was easily achieved by the RCN implementation.

The model block contains the real-time RCN implementation which involved implementing a sparse matrix multiplication algorithm necessary to deal with the highly sparse nature of the RCN design⁶⁸. Unlike `keras2c`-generated functions, the weights for the RCN were loaded as matrices to the PCS GUI and could therefore be changed during experiment to try out multiple models or retrain between experimental sessions. While other works have shown the possibility of retraining RCN type models intra-shot³⁷, this has yet to be implemented but remains a possibility for future work. The model block will output AE "amplitudes" or the likelihood of that AE type currently being present in the plasma. The 5 types of AEs that are detected are: Beta-induced AE, Ellipticity-induced AEs, low-frequency modes, reversed shear AEs (RSAEs), and Toroidal AEs (TAEs). Based on the offline frequency of occurrences and accuracy of the detector model, the model only passes the signal for TAEs and RSAEs to the controller block.

The controller block takes in the TAE and RSAE amplitudes and the user will decide which amplitude to use for feedback control as well as apply a low pass filter to smooth the RCN model outputs. The change in NBI power, ΔP_{NBI} , is calculated by $\Delta P_{NBI} = K_P \times (\text{Target}_{AE} - \text{Reference}_{AE})$ where K_P is the user-tuned proportional gain, Target_{AE} is the target AE amplitude, and Reference_{AE} is the RCN output amplitude. ΔP_{NBI} is then passed along to the NBI controller algorithm to adjust NBI duty cycles to achieve the requested NBI power target. There are limits to minimum and maximum P_{NBI} that constrain the controller as well as limits to the maximum rate of change of P_{NBI} to further constrain the controller as needed.

E. MPC Profile Control

An AI-based Model Predictive Controller (MPC) is implemented for plasma profile prediction and control. Data-driven plasma profile predictors have shown great promise in predicting the evolution of a discharge^{1,13}. These plasma models may be used for control through linearizing in the latent space and applying linear MPC^{53,71}. This control algorithm is implemented for multi-input multi-actuator profile control, and has been tested experimentally in DIII-D producing accurate rotation and density 33-point full profile control. A more detailed publication is found in Shousha et al.⁶⁶

The inputs for the profile controller model were the profiles provided by RTCAKENN, I_p , B_t , actuation hardware limits and the target profiles. The output of the controller block is NBI power and torque, ECH power and D2 gas injection voltage. The latent-space linearization encoder runs in 4ms, followed by the quadratic program (QP) solver for MPC taking up to 10ms, enabling a cycle time of 20ms.

The model block consists of an MLP keras2c-generated function that maps the RTCAKENN point profiles into a linear latent space whose size depends on the model training, but is typically around 10. The same mapping is applied to the user-input target profiles, producing a measured latent space and a target latent space.

The controller block uses the measured latent space, target latent space, I_p , B_t , actuator hardware limits and QP solver parameters and runs a QP optimization to output the optimal NBI power, torque, ECH power and gas voltage to reach the profile targets.

IV. CONCLUSION

The PACMAN algorithm provides a testing environment for novel ML-based models and controllers that leverage the diverse set of DIII-D diagnostic data to perform advanced real-time control. The input block provides basic diagnostic pre-processing to ensure adequate information without excessive constraints so ML models still have significant flexibility in their own normalizations and additional pre-processing. The model block allows for multiple types of ML model implementation with the opportunity for new model types to be developed and deployed in the future. The controller block takes the outputs from the various ML models and uses appropriate standard or advanced control techniques to produce actuator commands. Finally, the output block handles conflicts in actuator requests and ensures the tokamak's safety by imposing strict actuator constraints. The clear separation of each block eases the user design process and allows for the possibility of each block to be parallelized in the future.

The PACMAN framework has been demonstrated successfully in 5 listed experiments as well as an additional 4 not described in this manuscript: a divertor detachment controller¹⁴, an RL-based TM controller⁶⁴, a finite-state machine profile controller¹, and a previous RL β_N controller¹². The listed diverse experiments cover multiple types of model implementations utilizing keras2c for implementation of ML-based

survival models, non-linear encoders and RCN for event prediction models. There were different types of control as well including fully ML-based RL control, finite state machines, PID-based controllers, and advanced MPC controllers. The variability in model and controller types demonstrates PACMAN's flexibility to handle different control types and objectives that utilize the many diagnostics and actuators DIII-D has at its disposal.

In its current form, PACMAN is prepared for the inclusion of new models and controllers to achieve DIII-D future control milestones. The biggest future goal is to implement the multi-threading of the entire model and controller blocks to speed up the computation time of the full algorithm. Additionally, as new diagnostics and actuators come online, the inputs and output blocks will be adjusted to include those new control capabilities. Future work can also explore coupling GPU hardware or possibly FPGAs with PACMAN and the DIII-D PCS to further speed-up real-time inference speeds.

CREDIT STATEMENT

A. Rothstein: Lead Author. Design Lead. Manuscript Lead. TM Control Lead. AE Control Co-Lead.

H.J. Farre-Kaga: Lead Author. Design Lead. Profile Control Lead

J. Butt: ELM Predictor Lead. Design support. PCS Testing Lead.

R. Shousha: RTCAKENN Lead. Design Support. Paper editing.

K. Erickson: PCS Programming Lead.

T. Wakatsuki: RL ITB Lead.

A. Jalalvand: Design Support. AE Control Co-Lead. High-frequency diagnostics lead.

P. Steiner: Design Support. Paper editing.

S.K. Kim: Design Support.

E. Kolemen: Design Support. Supervision. Funding Support.

ACKNOWLEDGMENT

This material is based upon work supported by the U.S. Department of Energy, Office of Science, Office of Fusion Energy Sciences, using the DIII-D National Fusion Facility, a DOE Office of Science user facility, under Award DE-FC02-04ER54698. Additionally, this material is supported by the National Science Foundation Graduate Research Fellowship under Grant No. DGE-2039656 and by the U.S. Department of Energy, under Awards DE-SC0015480 and DE-AC02-09CH11466.

We would also like to thank David Eldon for insightful feedback on this manuscript.

DISCLAIMER

This report was prepared as an account of work sponsored by an agency of the United States Government. Neither the United States Government nor any agency thereof, nor any of their employees, makes any warranty, express or implied, or assumes any legal liability or responsibility for the accuracy, completeness, or usefulness of any information, apparatus, product, or process disclosed, or represents that its use would not infringe privately owned rights. Reference herein to any specific commercial product, process, or service by trade name, trademark, manufacturer, or otherwise does not necessarily constitute or imply its endorsement, recommendation, or favoring by the United States Government or any agency thereof. The views and opinions of authors expressed herein do not necessarily state or reflect those of the United States Government or any agency thereof.

REFERENCES

¹J. Abbate, R. Conlin, and E. Kolemen. Data-driven profile prediction for DIII-D. *Nuclear Fusion*, 61(4):046027, April 2021. ISSN 0029-5515, 1741-4326. doi:10.1088/1741-4326/abe08d. URL <https://iopscience.iop.org/article/10.1088/1741-4326/abe08d>.

²Joseph Abbate, Rory Conlin, Ricardo Shousha, Keith Erickson, and Egemen Kolemen. A general infrastructure for data-driven control design and implementation in tokamaks. *Journal of Plasma Physics*, 89(1):895890102, February 2023. ISSN 0022-3778, 1469-7807. doi:10.1017/S0022377822001040. URL https://www.cambridge.org/core/product/identifier/S0022377822001040/type/journal_article.

³Rushil Anirudh, Rick Archibald, M. Salman Asif, Markus M. Becker, Sadruddin Benkadda, Peer-Timo Bremer, Rick H. S. Budé, C. S. Chang, Lei Chen, R. M. Churchill, Jonathan Citrin, Jim A. Gaffney, Ana Gainaru, Walter Gekelman, Tom Gibbs, Satoshi Hamaguchi, Christian Hill, Kelli Humbird, Sören Jalas, Satoru Kawaguchi, Gon-Ho Kim, Manuel Kirchen, Scott Klasky, John L. Kline, Karl Krushelnick, Bogdan Kustowski, Giovanni Lapenta, Wenting Li, Tammy Ma, Nigel J. Mason, Ali Mesbah, Craig Michoski, Todd Munson, Izumi Murakami, Habib N. Najm, K. Erik J. Olofsson, Seolhye Park, J. Luc Peterson, Michael Probst, David Pugmire, Brian Sammuli, Kapil Sawlani, Alexander Scheinker, David P. Schissel, Rob J. Shalloo, Jun Shinagawa, Jaegu Seong, Brian K. Spears, Jonathan Tennyson, Jayaraman Thiagarajan, Catalin M. Ticoş, Jan Trieschmann, Jan Van Dijk, Brian Van Essen, Peter Ventzek, Haimin Wang, Jason T. L. Wang, Zhehui Wang, Kristian Wende, Xueqiao Xu, Hiroshi Yamada, Tatsuya Yokoyama, and Xinhua Zhang. 2022 Review of Data-Driven Plasma Science. *IEEE Transactions on Plasma Science*, 51(7):1750–1838, July 2023. ISSN 0093-3813, 1939-9375. doi:10.1109/TPS.2023.3268170. URL <https://ieeexplore.ieee.org/document/10214236/>.

⁴M. E. Austin and J. Lohr. Electron cyclotron emission radiometer upgrade on the DIII-D tokamak. *Review of Scientific Instruments*, 74(3):1457–1459, March 2003. ISSN 0034-6748. doi:10.1063/1.1530387. URL <https://doi.org/10.1063/1.1530387>. _eprint: https://pubs.aip.org/aip/rsi/article-pdf/74/3/1457/19084026/1457_1_online.pdf.

⁵J.L. Barr, B. Sammuli, D.A. Humphreys, E. Olofsson, X.D. Du, C. Rea, W.P. Wehner, M.D. Boyer, N.W. Eidiets, R. Granetz, A. Hyatt, T. Liu, N.C. Logan, S. Munaretto, E. Strait, Z.R. Wang, and The DIII-D Team. Development and experimental qualification of novel disruption prevention techniques on DIII-D. *Nuclear Fusion*, 61(12):126019, December 2021. ISSN 0029-5515, 1741-4326. doi:10.1088/1741-4326/ac2d56. URL <https://iopscience.iop.org/article/10.1088/1741-4326/ac2d56>.

⁶Mark D Boyer, Cristina Rea, and Mitchell D Clement. Toward active disruption avoidance via real-time estimation of the safe operat-

ing region and disruption proximity in tokamaks. *Nuclear Fusion*, November 2021. ISSN 0029-5515, 1741-4326. doi:10.1088/1741-4326/ac359e. URL <https://iopscience.iop.org/article/10.1088/1741-4326/ac359e>. tex.ids= boyer_toward_2021.

⁷M.D. Boyer, K.G. Erickson, B.A. Grierson, D.C. Pace, J.T. Scoville, J. Rauch, B.J. Crowley, J.R. Ferron, S.R. Haskey, D.A. Humphreys, R. Johnson, R. Nazikian, and C. Pawley. Feedback control of stored energy and rotation with variable beam energy and permeance on DIII-D. *Nuclear Fusion*, 59(7):076004, 2019. ISSN 0029-5515, 1741-4326. doi:10.1088/1741-4326/ab17f5. URL <https://iopscience.iop.org/article/10.1088/1741-4326/ab17f5>.

⁸J. Butt, H.J. Farre-Kaga, P. Steiner, X. Chen, T.H. Osborne, Q. Hu, K. Barada, K. Erickson, A. Rothstein, R. Shousha, T. Wilks, M. Austin, A. Bortolon, and E. Kolemen. Wide-pedestal qh mode pedestal evolution under predictive application of resonant 3d fields. Manuscript in preparation, 2025.

⁹R.J. Buttery, J.M. Park, J.T. McClenaghan, D. Weisberg, J. Canik, J. Ferron, A. Garofalo, C.T. Holcomb, J. Leuer, and P.B. Snyder. The advanced tokamak path to a compact net electric fusion pilot plant. *Nuclear Fusion*, 61(4):046028, April 2021. ISSN 0029-5515, 1741-4326. doi:10.1088/1741-4326/abe4af. URL <https://iopscience.iop.org/article/10.1088/1741-4326/abe4af>. tex.ids= buttery_advanced_2021-1, buttery_advanced_2021-2.

¹⁰Mirela Cengher, John Lohr, Paul Simmerling, Yuri Gorelov, Antonio Torrezan, Dan Ponce, John Doane, David Su, and Xi Chen. Status and Plans for the DIII-D ECH/ECCD System. *IEEE Transactions on Plasma Science*, 48(6):1698–1702, June 2020. ISSN 0093-3813, 1939-9375. doi:10.1109/TPS.2020.2978828. URL <https://ieeexplore.ieee.org/document/9046748/>.

¹¹Zhipeng Chang, Baofeng Gao, Ruijie Yin, and Xiaofei Zhao. DLTm: A deep learning method for tearing mode simulation and prediction. *Nuclear Fusion*, June 2025. ISSN 0029-5515, 1741-4326. doi:10.1088/1741-4326/ade891. URL <https://iopscience.iop.org/article/10.1088/1741-4326/ade891>.

¹²Ian Char, Joseph Abbate, Laszlo Bardoczi, Mark Boyer, Youngseog Chung, Rory Conlin, Keith Erickson, Viraj Mehta, Nathan Richner, Egemen Kolemen, and Jeff Schneider. Offline model-based reinforcement learning for tokamak control. In Nikolai Matni, Manfred Morari, and George J. Pappas, editors, *Proceedings of The 5th Annual Learning for Dynamics and Control Conference*, volume 211 of *Proceedings of Machine Learning Research*, pages 1357–1372. PMLR, 15–16 Jun 2023. URL <https://proceedings.mlr.press/v211/char23a.html>.

¹³Ian Char, Youngseog Chung, Joseph Abbate, Egemen Kolemen, and Jeff Schneider. Full Shot Predictions for the DIII-D Tokamak via Deep Recurrent Networks, April 2024. URL <http://arxiv.org/abs/2404.12416> [physics].

¹⁴N. Chen, C.S. Byun, A. Jalalvand, S.K. Kim, A. Rothstein, F. Scotti, S. Allen, D. Eldon, K. Erickson, and E. Kolemen. Regulation compliant ai for fusion: Real-time image analysis-based control of divertor detachment in tokamaks. Manuscript under submission., 2025.

¹⁵C. Chrystal, K. H. Burrell, B. A. Grierson, S. R. Haskey, R. J. Groebner, D. H. Kaplan, and A. Briesemeister. Improved edge charge exchange recombination spectroscopy in DIII-D. *Review of Scientific Instruments*, 87(11):11E512, November 2016. ISSN 0034-6748, 1089-7623. doi:10.1063/1.4958915. URL <https://pubs.aip.org/rsi/article/87/11/11E512/362651/Improved-edge-charge-exchange-recombination>.

¹⁶Rory Conlin, Keith Erickson, Joseph Abbate, and Egemen Kolemen. Keras2c: A library for converting Keras neural networks to real-time compatible C. *Engineering Applications of Artificial Intelligence*, 100:104182, April 2021. ISSN 09521976. doi:10.1016/j.engappai.2021.104182. URL <https://linkinghub.elsevier.com/retrieve/pii/S0952197621000294>.

¹⁷A. J. Creely, M. J. Greenwald, S. B. Ballinger, D. Brunner, J. Canik, J. Doody, T. Fülop, D. T. Garnier, R. Granetz, T. K. Gray, C. Holland, N. T. Howard, J. W. Hughes, J. H. Irby, V. A. Izzo, G. J. Kramer, A. Q. Kuang, B. LaBombard, Y. Lin, B. Lipschultz, N. C. Logan, J. D. Lore, E. S. Marmor, K. Montes, R. T. Mumgaard, C. Paz-Soldan, C. Rea, M. L. Reinke, P. Rodriguez-Fernandez, K. Särkinäki, F. Sciortino, S. D. Scott, A. Snicker, P. B. Snyder, B. N. Sorbom, R. Sweeney, R. A. Tinguely,

E. A. Tolman, M. Umansky, O. Vallhagen, J. Varje, D. G. Whyte, J. C. Wright, S. J. Wukitch, J. Zhu, and the SPARC Team. Overview of the SPARC tokamak. *Journal of Plasma Physics*, 86(5):865860502, October 2020. ISSN 0022-3778, 1469-7807. doi:10.1017/S0022377820001257. URL https://www.cambridge.org/core/product/identifier/S0022377820001257/type/journal_article.

¹⁸A. J. Creely, D. Brunner, R. T. Mumgaard, M. L. Reinke, M. Segal, B. N. Sorbom, and M. J. Greenwald. SPARC as a platform to advance tokamak science. *Physics of Plasmas*, 30(9):090601, September 2023. ISSN 1070-664X, 1089-7674. doi:10.1063/5.0162457. URL <https://pubs.aip.org/pop/article/30/9/090601/2909870/SPARC-as-a-platform-to-advance-tokamak-science>.

¹⁹G. De Tommasi, S. Dubbioso, Y. Huang, Z. P. Luo, A. Mele, and B. J. Xiao. A RL-based Vertical Stabilization System for the EAST tokamak. In *2022 American Control Conference (ACC)*, pages 5328–5333, Atlanta, GA, USA, June 2022. IEEE. ISBN 978-1-6654-5196-3. doi:10.23919/ACC53348.2022.9867499. URL <https://ieeexplore.ieee.org/document/9867499/>.

²⁰P.C. De Vries, M. Cinque, G. De Tommasi, W. Treutterer, D. Humphreys, M. Walker, F. Felici, I. Gomez, L. Zabeo, T. Ravensbergen, L. Pangione, F. Rimini, S. Rosiello, Y. Gribov, M. Dubrov, A. Vu, I. Carvalho, W.R. Lee, T. Tak, A. Zagar, R. Gunion, R. Pitts, M. Mattei, A. Pironti, M. Arriola, F. Pesamosca, O. Kudlacek, G. Raupp, G. Pautasso, R. Nouailletas, Ph. Moreau, and D. Weldon. Strategy to systematically design and deploy the ITER plasma control system: A system engineering and model-based design approach. *Fusion Engineering and Design*, 204:114464, July 2024. ISSN 09203796. doi:10.1016/j.fusengdes.2024.114464. URL <https://linkinghub.elsevier.com/retrieve/pii/S0920379624004915>.

²¹Jonas Degrave, Federico Felici, Jonas Buchli, Michael Neunert, Brendan Tracey, Francesco Carpanese, Timo Ewalds, Roland Hafner, Abbas Abdolmaleki, Diego De Las Casas, Craig Donner, Leslie Fritz, Cristian Galperti, Andrea Huber, James Keeling, Maria Tsimpoukelli, Jackie Kay, Antoine Merle, Jean-Marc Moret, Seb Noury, Federico Pesamosca, David Pfau, Olivier Sauter, Cristian Sommariva, Stefano Coda, Basil Duval, Ambrogio Fasoli, Pushmeet Kohli, Koray Kavukcuoglu, Demis Hassabis, and Martin Riedmiller. Magnetic control of tokamak plasmas through deep reinforcement learning. *Nature*, 602(7897):414–419, February 2022. ISSN 0028-0836, 1476-4687. doi:10.1038/s41586-021-04301-9. URL <https://www.nature.com/articles/s41586-021-04301-9>.

²²S. Dubbioso, G. De Tommasi, A. Mele, G. Tartaglione, M. Arriola, and A. Pironti. A Deep Reinforcement Learning approach for Vertical Stabilization of tokamak plasmas. *Fusion Engineering and Design*, 194:113725, September 2023. ISSN 09203796. doi:10.1016/j.fusengdes.2023.113725. URL <https://linkinghub.elsevier.com/retrieve/pii/S0920379623003083>.

²³T.E. Evans, M.E. Fenstermacher, R.A. Moyer, T.H. Osborne, J.G. Watkins, P. Ghohil, I. Joseph, M.J. Schaffer, L.R. Baylor, M. Bécoulet, J.A. Boedo, K.H. Burrell, J.S. deGrassie, K.H. Finken, T. Jernigan, M.W. Jakubowski, C.J. Lasnier, M. Lehnert, A.W. Leonard, J. Lonnroth, E. Nardon, V. Parail, O. Schmitz, B. Unterberg, and W.P. West. RMP ELM suppression in DIII-D plasmas with ITER similar shapes and collisionalities. *Nuclear Fusion*, 48(2):024002, January 2008. doi:10.1088/0029-5515/48/2/024002. URL <https://dx.doi.org/10.1088/0029-5515/48/2/024002>.

²⁴H.J. Farre-Kaga, A. Rothstein, R. Sonker, S.K. Kim, R. Shousha, M.S. Kim, K. Erickson, J. Schneider, and E. Kolemen. Interpreting ai for fusion: An application to plasma profile analysis for tearing mode stability. Manuscript under submission., 2025.

²⁵F. Felici and O. Sauter. Non-linear model-based optimization of actuator trajectories for tokamak plasma profile control. *Plasma Physics and Controlled Fusion*, 54(2):025002, February 2012. ISSN 0741-3335, 1361-6587. doi:10.1088/0741-3335/54/2/025002. URL <https://iopscience.iop.org/article/10.1088/0741-3335/54/2/025002>.

²⁶J.R. Ferron, M.L. Walker, L.L. Lao, H.E. St John, D.A. Humphreys, and J.A. Leuer. Real time equilibrium reconstruction for tokamak discharge control. *Nuclear Fusion*, 38(7):1055–1066, July 1998. ISSN 0029-5515. doi:10.1088/0029-5515/38/7/308. URL <https://iopscience.iop.org/article/10.1088/0029-5515/38/7/308>.

²⁷Yichen Fu, David Eldon, Keith Erickson, Kornee Kleijwegt, Leonard Lupin-Jimenez, Mark D. Boyer, Nick Eidietis, Nathaniel Barbour, Olivier Izacard, and Egemen Kolemen. Machine learning control for disruption and tearing mode avoidance. *Physics of Plasmas*, 27(2):022501, February 2020. ISSN 1070-664X. doi:10.1063/1.5125581. URL <https://doi.org/10.1063/1.5125581>. eprint: https://pubs.aip.org/aip/pop/article-pdf/doi/10.1063/1.5125581/19788998/022501_1_online.pdf.

²⁸Cristian Galperti, Federico Felici, Trang Vu, Olivier Sauter, F. Carpanese, M. Kong, G. Marcea, A. Merle, A. Pau, A. Perek, F. Pesamosca, M. Baquero-Ruiz, S. Coda, J. Decker, B. Duval, M. Gospodarczyk, A. Karpushov, S. Marchionni, A. Maier, B. Marletaz, A. Segovia, B. Vincent, C. Yildiz, D. Carnevale, N. Ferron, J. Koenders, B. Kool, G. Manduchi, M. Maraschek, P. Milne, A.C. Neto, E. Poli, T. Ravensbergen, M. Reich, N. Rispoli, and F. Sartori. Overview of the TCV digital real-time plasma control system and its applications. *Fusion Engineering and Design*, 208:114640, November 2024. ISSN 09203796. doi:10.1016/j.fusengdes.2024.114640. URL <https://linkinghub.elsevier.com/retrieve/pii/S0920379624004915>.

²⁹B H Guo, B Shen, D L Chen, C Rea, R S Granetz, Y Huang, L Zeng, H Zhang, J P Qian, Y W Sun, and B J Xiao. Disruption prediction using a full convolutional neural network on EAST. *Plasma Physics and Controlled Fusion*, 63(2):025008, February 2021. ISSN 0741-3335, 1361-6587. doi:10.1088/1361-6587/abcbab. URL <https://iopscience.iop.org/article/10.1088/1361-6587/abcbab>.

³⁰Anchal Gupta, David Eldon, Eunnam Bang, KyuBeen Kwon, Hyungho Lee, Anthony Leonard, Junghoo Hwang, Xueqiao Xu, Menglong Zhao, and Ben Zhu. Detachment control in KSTAR with Tungsten divertor, May 2025. URL <http://arxiv.org/abs/2505.07978>. arXiv:2505.07978 [physics].

³¹Sang-hee Hahn, H. Han, M.H. Woo, J.G. Bak, J. Chung, Y.M. Jeon, J.H. Jeong, M. Joung, J.W. Juhn, H.S. Kim, Heungsu Kim, M.W. Lee, G.W. Shin, T.H. Tak, S.W. Yoon, J. Barr, N.W. Eidietis, D.A. Humphreys, A. Hyatt, B.G. Penaflor, D.A. Piglowski, M.L. Walker, A.S. Welander, M.D. Boyer, K. Erickson, and D. Mueller. Advances and challenges in KSTAR plasma control toward long-pulse, high-performance experiments. *Fusion Engineering and Design*, 156:111622, July 2020. ISSN 09203796. doi:10.1016/j.fusengdes.2020.111622. URL <https://linkinghub.elsevier.com/retrieve/pii/S0920379620301708>.

³²A. Hassanein and V. Sizyuk. Potential design problems for ITER fusion device. *Scientific Reports*, 11(1):2069, January 2021. ISSN 2045-2322. doi:10.1038/s41598-021-81510-2. URL <https://www.nature.com/articles/s41598-021-81510-2>.

³³A. Hassanein, T. Sizyuk, and M. Ulrickson. Vertical displacement events: A serious concern in future ITER operation. *Fusion Engineering and Design*, 83(7-9):1020–1024, December 2008. ISSN 09203796. doi:10.1016/j.fusengdes.2008.05.032. URL <https://linkinghub.elsevier.com/retrieve/pii/S0920379608001166>.

³⁴C. T. Holcomb, S. L. Allen, M. A. Makowski, R. J. Jayakumar, M. F. Gu, S. Lerner, K. L. Morris, J. Latkowski, J. M. Moller, W. Meyer, R. Ellis, R. Geer, D. Behne, R. Chipman, P. Smith, S. McClain, Giuseppe Gorini, Francesco P. Orsitta, Elio Sindoni, and Marco Tardocchi. An Overview Of The Motional Stark Effect Diagnostic On DIII-D And Design Work For An ITER MSE. In *AIP Conference Proceedings*, volume 988, pages 214–217, Varenna (Italy), 2008. AIP. doi:10.1063/1.2905070. URL <https://pubs.aip.org/aip/acp/article/988/1/214-217/604716>. ISSN: 0094243X.

³⁵W.H. Hu, C. Rea, Q.P. Yuan, K.G. Erickson, D.L. Chen, B. Shen, Y. Huang, J.Y. Xiao, J.J. Chen, Y.M. Duan, Y. Zhang, H.D. Zhuang, J.C. Xu, K.J. Montes, R.S. Granetz, L. Zeng, J.P. Qian, B.J. Xiao, and J.G. Li. Real-time prediction of high-density EAST disruptions using random forest. *Nuclear Fusion*, 61(6):066034, June 2021. ISSN 0029-5515, 1741-4326. doi:10.1088/1741-4326/abf74d. URL <https://iopscience.iop.org/article/10.1088/1741-4326/abf74d>.

³⁶Yao Huang, B.J. Xiao, Z.P. Luo, Q.P. Yuan, X.F. Pei, and X.N. Yue. Implementation of GPU parallel equilibrium reconstruction for plasma control in EAST. *Fusion Engineering and Design*, 112:1019–1024, November 2016. ISSN 09203796. doi:10.1016/j.fusengdes.2016.02.048. URL <https://linkinghub.elsevier.com/retrieve/pii/S0920379616301302>.

³⁷Azarakhsh Jalavand, Joseph Abbate, Rory Conlin, Geert Verdoollaeghe, and Egemen Kolemen. Real-time and Adaptive Reservoir Computing with Application to Profile Prediction in Fusion Plasma. *IEEE TRANSACTIONS ON NEURAL NETWORKS AND LEARNING SYSTEMS*, page 12, 2021.

³⁸Azarakhsh Jalavand, Alan A. Kaptanoglu, Alvin V. Garcia, Andrew O. Nelson, Joseph Abbate, Max E. Austin, Geert Verdoollaeghe, Steven L. Brunton, William W. Heidbrink, and Egemen Kolemen. Alfvén eigenmode classification based on ECE diagnostics at DIII-D using deep recurrent neural networks. *Nuclear Fusion*, 62(2):026007, February 2022. ISSN 0029-5515, 1741-4326. doi:10.1088/1741-4326/ac3be7. URL <https://iopscience.iop.org/article/10.1088/1741-4326/ac3be7>. Publisher: IOP Publishing.

³⁹S. K. Kim, R. Shousha, S. M. Yang, Q. Hu, S. H. Hahn, A. Jalavand, J.-K. Park, N. C. Logan, A. O. Nelson, Y.-S. Na, R. Nazikian, R. Wilcox, R. Hong, T. Rhodes, C. Paz-Soldan, Y. M. Jeon, M. W. Kim, W. H. Ko, J. H. Lee, A. Battey, G. Yu, A. Bortolon, J. Snipes, and E. Kolemen. Highest fusion performance without harmful edge energy bursts in tokamak. *Nature Communications*, 15(1):3990, May 2024. ISSN 2041-1723. doi:10.1038/s41467-024-48415-w. URL <https://www.nature.com/articles/s41467-024-48415-w>.

⁴⁰E. Kolemen, R. Ellis, R.J. La Haye, D.A. Humphreys, J. Lohr, S. Noraky, B.G. Penaflor, and A.S. Welander. Real-time mirror steering for improved closed loop neoclassical tearing mode suppression by electron cyclotron current drive in DIII-D. *Fusion Engineering and Design*, 88(11):2757–2760, November 2013. ISSN 09203796. doi:10.1016/j.fusengdes.2013.02.168. URL <https://linkinghub.elsevier.com/retrieve/pii/S0920379613002834>.

⁴¹O. Kudlacek, P. David, I. Gomez, A. Gräter, B. Sieglin, W. Treutterer, M. Weiland, T. Zeherbauer, M. Van Berkel, M. Bernert, T. Bosman, F. Felici, L. Giannone, J. Illerhaus, D. Kropackova, P.T. Lang, M. Maraschek, B. Ploeckl, M. Reich, A. Vedl Kubincova, the ASDEX Upgrade Team, and EUROfusion Tokamak Exploitation Team. Overview of advances in ASDEX Upgrade plasma control to support critical physics research for ITER and beyond. *Nuclear Fusion*, 64(5):056012, May 2024. ISSN 0029-5515, 1741-4326. doi:10.1088/1741-4326/ad3472. URL <https://iopscience.iop.org/article/10.1088/1741-4326/ad3472>.

⁴²Hoang-Bao Le, Basil P. Duval, Jean-Marc Moret, and N. Cruz. New developments for real time plasma control system of TCV Tokamak based on FPGA. In *2014 19th IEEE-NPSS Real Time Conference*, pages 1–2, Nara, Japan, May 2014. IEEE. ISBN 978-1-4799-3659-5. doi:10.1109/RTC.2014.7097426. URL <https://ieeexplore.ieee.org/document/7097426/>.

⁴³M. Lennholm, T. Budd, R. Felton, M. Gadeberg, A. Goodyear, F. Milani, and F. Sartori. Plasma control at JET. *Fusion Engineering and Design*, 48(1-2):37–45, August 2000. ISSN 09203796. doi:10.1016/S0920-3796(00)00125-3. URL <https://linkinghub.elsevier.com/retrieve/pii/S0920379600001253>.

⁴⁴M. Margo, B. Penaflor, H. Shen, J. Ferron, D. Piglowski, P. Nguyen, J. Rauch, M. Clement, A. Battey, and C. Rea. Current State of DIII-D Plasma Control System. *Fusion Engineering and Design*, 150:111368, January 2020. ISSN 09203796. doi:10.1016/j.fusengdes.2019.111368. URL <https://linkinghub.elsevier.com/retrieve/pii/S0920379619308646>.

⁴⁵K.J. Montes, C. Rea, R.S. Granetz, R.A. Tinguely, N. Eidietis, O.M. Meneghini, D.L. Chen, B. Shen, B.J. Xiao, K. Erickson, and M.D. Boyer. Machine learning for disruption warnings on Alcator C-Mod, DIII-D, and EAST. *Nuclear Fusion*, 59(9):096015, September 2019. ISSN 0029-5515, 1741-4326. doi:10.1088/1741-4326/ab1df4. URL <https://iopscience.iop.org/article/10.1088/1741-4326/ab1df4>.

⁴⁶J.-M. Moret, B.P. Duval, H.B. Le, S. Coda, F. Felici, and H. Reimerdes. Tokamak equilibrium reconstruction code LIUQE and its real time implementation. *Fusion Engineering and Design*, 91:1–15, February 2015. ISSN 09203796. doi:10.1016/j.fusengdes.2014.09.019. URL <https://linkinghub.elsevier.com/retrieve/pii/S0920379614005973>.

⁴⁷S. Morosohk, B. Leard, T. Rafiq, and E. Schuster. Machine learning enhanced model-based scenario optimization for DIII-D. *Nuclear Fusion*, 64(5):056018, May 2024. ISSN 0029-5515, 1741-4326. doi:10.1088/1741-4326/ad35d6. URL <https://iopscience.iop.org/article/10.1088/1741-4326/ad35d6>.

⁴⁸Shira Morosohk and Eugenio Schuster. Real-time estimation of the electron temperature profile in DIII-D by leveraging neural-network surrogate models. *Contributions to Plasma Physics*, 63(5-6):e202200153, June 2023. ISSN 0863-1042, 1521-3986. doi:10.1002/ctpp.202200153. URL <https://onlinelibrary.wiley.com/doi/10.1002/ctpp.202200153>.

⁴⁹Shira Morosohk, Andres Pajares, and Eugenio Schuster. Estimation of the Electron Temperature Profile in Tokamaks Using Analytical and Neural Network Models. In *2022 American Control Conference (ACC)*, pages 278–283, Atlanta, GA, USA, June 2022. IEEE. ISBN 978-1-6654-5196-3. doi:10.23919/ACC53348.2022.9867844. URL <https://ieeexplore.ieee.org/document/9867844/>.

⁵⁰Shira M. Morosohk, Mark D. Boyer, and Eugenio Schuster. Accelerated version of NUBEAM capabilities in DIII-D using neural networks. *Fusion Engineering and Design*, 163:112125, February 2021. ISSN 09203796. doi:10.1016/j.fusengdes.2020.112125. URL <https://linkinghub.elsevier.com/retrieve/pii/S0920379620306736>.

⁵¹S.M. Morosohk, A. Pajares, T. Rafiq, and E. Schuster. Neural network model of the multi-mode anomalous transport module for accelerated transport simulations. *Nuclear Fusion*, 61(10):106040, October 2021. ISSN 0029-5515, 1741-4326. doi:10.1088/1741-4326/ac207e. URL <https://iopscience.iop.org/article/10.1088/1741-4326/ac207e>.

⁵²Chirag Nagpal, Willa Potosnak, and Artur Dubrawski. auton-survival: an open-source package for regression, counterfactual estimation, evaluation and phenotyping with censored time-to-event data. In Zachary Lipton, Rakesh Ranganath, Mark Sendak, Michael Sjoding, and Serena Yeung, editors, *Proceedings of the 7th Machine Learning for Healthcare Conference*, volume 182 of *Proceedings of Machine Learning Research*, pages 585–608. PMLR, 05–06 Aug 2022. URL <https://proceedings.mlr.press/v182/nagpal22a.html>.

⁵³Samuel E. Otto and Clarence W. Rowley. Linearly recurrent autoencoder networks for learning dynamics. *SIAM Journal on Applied Dynamical Systems*, 18(1):558–593, 2019. doi:10.1137/18M1177846. URL <https://doi.org/10.1137/18M1177846>.

⁵⁴C.J. Pawley, B.J. Crowley, D.C. Pace, J.M. Rauch, J.T. Scoville, D.H. Kellman, and A.G. Kellman. Advanced control of neutral beam injected power in DIII-D. *Fusion Engineering and Design*, 123:453–457, November 2017. ISSN 09203796. doi:10.1016/j.fusengdes.2017.02.106. URL <https://linkinghub.elsevier.com/retrieve/pii/S0920379617301990>.

⁵⁵Piotr Perek, Taehyun Tak, Woong-Ryol Lee, Anze Zagari, Dariusz Makowski, Domen Soklic, and Peter Karlovsek. Preliminary design of ITER PCS Provisioning System. *Fusion Engineering and Design*, 220:115348, November 2025. ISSN 09203796. doi:10.1016/j.fusengdes.2025.115348. URL <https://linkinghub.elsevier.com/retrieve/pii/S0920379625005447>.

⁵⁶E. Poli, A. Bock, M. Lochbrunner, O. Maj, M. Reich, A. Snicker, A. Stegmeir, F. Volpe, N. Bertelli, R. Bilato, G.D. Conway, D. Farina, F. Felici, L. Figini, R. Fischer, C. Galperti, T. Happel, Y.R. Lin-Liu, N.B. Marushchenko, U. Mszanowski, F.M. Poli, J. Stober, E. Westerhof, R. Zille, A.G. Peeters, and G.V. Pereverzev. TORBEAM 2.0, a paraxial beam tracing code for electron-cyclotron beams in fusion plasmas for extended physics applications. *Computer Physics Communications*, 225:36–46, April 2018. ISSN 00104655. doi:10.1016/j.cpc.2017.12.018. URL <https://linkinghub.elsevier.com/retrieve/pii/S001046551730423X>.

⁵⁷D. M. Ponce-Marquez, B. D. Bray, T. M. Deterly, C. Liu, and D. Eldon. Thomson scattering diagnostic upgrade on DIII-D. *Review of Scientific Instruments*, 81(10):10D525, October 2010. ISSN 0034-6748, 1089-7623. doi:10.1063/1.3495759. URL <https://pubs.aip.org/rsi/article/81/10/10D525/354675/Thomson-scattering-diagnostic-upgrade-on-DIII-Da>.

⁵⁸N. Rath, J. Bialek, P.J. Byrne, B. DeBono, J.P. Levesque, B. Li, M.E. Mauel, D.A. Maurer, G.A. Navratil, and D. Shiraki. High-speed, multi-input, multi-output control using GPU processing in the HBT-EP tokamak. *Fusion Engineering and Design*, 87(12):1895–1899, December 2012. ISSN 09203796. doi:10.1016/j.fusengdes.2012.04.003. URL <https://linkinghub.elsevier.com/retrieve/pii/S0920379612002542>.

⁵⁹N Rath, S Angelini, J Bialek, P J Byrne, B DeBono, P Hughes, J P Levesque, M E Mauel, G A Navratil, Q Peng, D Rhodes, and C Stofer. Adaptive control of rotating magnetic perturbations in HBT-EP using GPU processing. *Plasma Physics and Controlled Fusion*, 55(8):084003, August 2013. ISSN 0741-3335, 1361-6587. doi:10.1088/0741-3335/55/8/084003. URL <https://iopscience.iop.org/article/10.1088/0741-3335/55/8/084003>.

⁶⁰C. Rea, K.J. Montes, K.G. Erickson, R.S. Granetz, and R.A. Tinguely. A real-time machine learning-based disruption predictor in DIII-D. *Nuclear Fusion*, 59(9):096016, September 2019. ISSN 0029-5515, 1741-4326. doi:10.1088/1741-4326/ab28bf. URL <https://iopscience.iop.org/article/10.1088/1741-4326/ab28bf>.

⁶¹A. Rothstein, H.J. Farre-Kaga, and E. Kolemen. Preemptive tearing mode stabilization with multi-tasking ech. Manuscript in preparation., 2025.

⁶²Andrew Rothstein, Azarakhsh Jalalvand, Joseph Abbate, Keith Erickson, and Egemen Kolemen. Initial testing of Alfvén eigenmode feedback control with machine-learning observers on DIII-D. *Nuclear Fusion*, 64(9):096020, September 2024. ISSN 0029-5515, 1741-4326. doi:10.1088/1741-4326/ad64e6. URL <https://iopscience.iop.org/article/10.1088/1741-4326/ad64e6>.

⁶³Andrew Rothstein, Minseok Kim, Minho Woo, Minsoo Cha, Cheolsik Byun, Sangkyeun Kim, Keith Erickson, Youngho Lee, Josh Josephy-Zack, Jalal Butt, Ricardo Shousha, Mi Joung, June-Woo Juhn, Kyu-Dong Lee, and Egemen Kolemen. TorbeamNN: machine learning-based steering of ECH mirrors on KSTAR. *Plasma Physics and Controlled Fusion*, 67(5):055036, May 2025. ISSN 0741-3335, 1361-6587. doi:10.1088/1361-6587/add08b. URL <https://iopscience.iop.org/article/10.1088/1361-6587/add08b>.

⁶⁴Jaemin Seo, SangKyeun Kim, Azarakhsh Jalalvand, Rory Conlin, Andrew Rothstein, Joseph Abbate, Keith Erickson, Josiah Wai, Ricardo Shousha, and Egemen Kolemen. Avoiding fusion plasma tearing instability with deep reinforcement learning. *Nature*, 626(8000):746–751, February 2024. ISSN 0028-0836, 1476-4687. doi:10.1038/s41586-024-07024-9. URL <https://www.nature.com/articles/s41586-024-07024-9>.

⁶⁵R. Shousha, S. K. Kim, K. G. Erickson, S. H. Hahn, A. O. Nelson, S. M. Yang, J.-K. Park, J. Wai, Y. M. Jeon, J. H. Lee, J. Jang, D. Seo, and E. Kolemen. Design and experimental demonstration of feedback adaptive RMP ELM controller toward complete long pulse ELM suppression on KSTAR. *Physics of Plasmas*, 29(3):032514, March 2022. ISSN 1070-664X, 1089-7674. doi:10.1063/5.0081928. URL <https://pubs.aip.org/pop/article/29/3/032514/2847869/Design-and-experimental-demonstration-of-feedback>. Publisher: AIP Publishing.

⁶⁶R. Shousha, H. Farre-Kaga, P. Steiner, A. Rothstein, J. Seo, S. Kim, K. Erickson, A. Jalalvand, and E. Kolemen. Real-time ai enables closed-loop control of unmeasured tokamak profiles. Manuscript in preparation, Princeton Plasma Physics Laboratory and DIII-D National Fusion Facility, 2025, 2025.

⁶⁷Ricardo Shousha, Jaemin Seo, Keith Erickson, Zichuan Xing, SangKyeun Kim, Joseph Abbate, and Egemen Kolemen. Machine learning-based real-time kinetic profile reconstruction in DIII-D. *Nuclear Fusion*, 64(2):026006, 2023. ISSN 0029-5515, 1741-4326. doi:10.1088/1741-4326/ad142f. URL <https://iopscience.iop.org/article/10.1088/1741-4326/ad142f>. Publisher: IOP Publishing.

⁶⁸Gouhei Tanaka, Toshiyuki Yamane, Jean Benoit Héroux, Ryosho Nakane, Naoki Kanazawa, Seiji Takeda, Hidetoshi Numata, Daiju Nakano, and Akira Hirose. Recent advances in physical reservoir computing: A review. *Neural Networks*, 115:100–123, July 2019. ISSN 08936080. doi:10.1016/j.neunet.2019.03.005. URL <https://linkinghub.elsevier.com/retrieve/pii/S0893608019300784>.

⁶⁹T. Wakatsuki. Control of itbs in high q_{min} plasmas. Manuscript in preparation., 2025.

⁷⁰T. Wakatsuki, T. Suzuki, N. Hayashi, N. Oyama, and S. Ide. Safety factor profile control with reduced central solenoid flux consumption during plasma current ramp-up phase using a reinforcement learning technique. *Nuclear Fusion*, 59(6):066022, June 2019. ISSN 0029-5515, 1741-4326. doi:10.1088/1741-4326/ab1571. URL <https://iopscience.iop.org/article/10.1088/1741-4326/ab1571>.

⁷¹Manuel Watter, Jost Tobias Springenberg, Joschka Boedecker, and Martin Riedmiller. Embed to Control: A Locally Linear Latent Dynamics Model for Control from Raw Images, November 2015. URL <http://arxiv.org/abs/1506.07365>. arXiv:1506.07365 [cs].

⁷²Y. Wei, R. F. Forelli, C. Hansen, J. P. Levesque, N. Tran, J. C. Agar, G. Di Guglielmo, M. E. Mael, and G. A. Navratil. Low latency optical-based mode tracking with machine learning deployed on FPGAs on a tokamak. *Review of Scientific Instruments*, 95(7):073509, July 2024. ISSN 0034-6748, 1089-7623. doi:10.1063/5.0190354. URL <https://pubs.aip.org/rsi/article/95/7/073509/3302456/Low-latency-optical-based-mode-tracking-with>.

⁷³L.L. Yan, Q.P. Yuan, B.J. Xiao, R.R. Zhang, Y.Y. Zheng, J.Q. Zhu, and H.R. Guo. Custom application of PCS software development platform on EAST. *Fusion Engineering and Design*, 166:112314, May 2021. ISSN 09203796. doi:10.1016/j.fusengdes.2021.112314. URL <https://linkinghub.elsevier.com/retrieve/pii/S0920379621000909>.

⁷⁴I. Yonekawa, Y. Kawamata, T. Totsuka, H. Akasaka, M. Sueoka, and H. Yoshida. Current status and future prospects of the JT-60U control system. *Fusion Engineering and Design*, 71(1-4):11–15, June 2004. ISSN 09203796. doi:10.1016/j.fusengdes.2004.04.003. URL <https://linkinghub.elsevier.com/retrieve/pii/S0920379604000158>.

⁷⁵Hartmut Zohm. Assessment of DEMO challenges in technology and physics. *Fusion Engineering and Design*, 88(6-8):428–433, October 2013. ISSN 09203796. doi:10.1016/j.fusengdes.2013.01.001. URL <https://linkinghub.elsevier.com/retrieve/pii/S0920379613000021>.

V. APPENDIX

A. ML Controller Planning

Before exploring the controller examples that have been deployed in experiment using the PACMAN framework, we will provide a summary of important points within the PACMAN framework that are relevant for a real-time experimentalist designing and implementing a ML model for real-time plasma control. This is also relevant for exploring other non-CPU based implementations of ML models as similar design considerations will come into play.

The real-time implementation design process must begin before any ML model is trained in order to achieve the best success. Without prior consideration of these design decisions, the experimentalist will likely need to retrain their model from scratch or make significant changes to their control scheme. The experimentalist should have, at minimum, the following considerations:

- What is the control objective? What timescale does this control objective evolve on? Is this compatible with approximate timescales for real-time ML models?
- What actuators will be used to reach this control objective? What timescale do my actuator need to change to achieve this target?
- What inputs will the ML model use? What is the sim-to-real gap between the real-time data and the offline training data? How can that sim-to-real gap be minimized? How quickly does the model need to run to achieve my control objectives?
- What type of control scheme will be used with the ML model? Does this controller know about actuator limits and actuator failures?

Utilizing the PACMAN framework provides some basic answers to some of these questions in order to guide a novice interested in deploying a real-time control algorithm. The main forced answers come into play by imposing limits to timescales, forcing all model evaluation, control actuation,

and control objective timescales to be on the order of milliseconds or longer for control and objective timescales. While this is insufficient for all plasma control applications, the PACMAN

framework covers the vast majority of relevant timescales and enables ease of deployment for a significant number of ML models and controllers.